

(Fig. 4A). In contrast, *Delta1*, *Hes-1*, and *Notch1*, 2, 3, and 4 expression levels and cellular localization of *Hes-1* appeared unaffected [Fig. 4A and Web fig. 4 (14)]. These observations are consistent with previous findings that *Math1* is upstream of *NeuroD* (27) and the notion that *Math1* has a positive feedback effect on Notch ligand (e.g., *Delta3*) expression.

Our findings provide new insight into the role of Notch-mediated lateral inhibition in controlling differentiation of intestinal epithelial lineages. Building on the model set forth by Bjerknes and Cheng (8), we propose that a single self-maintaining stem cell gives rise to two daughter cells directly or through intermediate progenitors (Fig. 4B). In one daughter cell, interaction between Delta and Notch homologs elevates *Hes1* expression, inhibiting *Math1* expression, and this cell adopts an enterocyte fate. In the other daughter cell, lack of *Hes1* expression increases *Math1* expression, and this cell becomes a committed multipotent progenitor that will differentiate into a secretory lineage cell (Fig. 4B). Further differentiation of the secretory lineage into goblet, enteroendocrine, and Paneth cells requires other factors. *NeuroD* has been shown to play a role in differentiation of the secretin and cholecystokinin enteroendocrine cells (24); early committed multipotent endocrine cells can branch into at least three lineages (Fig. 4B) (24). *Rac1* is reported to play a positive role in goblet and Paneth cell differentiation but does not seem to have any impact on the enteroendocrine lineage (18), suggesting that goblet and Paneth cells share a closer relationship during later development. Constitutively activated *Rac1* causes precocious enterocyte growth, indicating its positive role in the absorptive cell lineage (18). These observations suggest that there is cross talk between the Notch and Rho GTPase pathways during formation of the gut epithelium. We cannot yet rule out other models for controlling the secretory and absorptive lineages: e.g., instead of arising from one *Math1*-positive progenitor, the goblet, enteroendocrine, and Paneth cells may differentiate from three distinct progenitors that each express *Math1*. Further study of *Math1* in the mouse intestine will yield deeper insight into the mechanisms controlling production of the different cell types, which may in turn provide therapeutic tools for endocrine and colorectal cancers and regeneration of the intestinal epithelium after injury.

References and Notes

1. H. Cheng, C. P. Leblond, *Am. J. Anat.* **141**, 537 (1974).  
 2. J. I. Gordon, G. H. Schmidt, K. A. Roth, *FASEB J.* **6**, 3039 (1992).  
 3. S. P. Bach, A. G. Renehan, C. S. Potten, *Carcinogenesis* **21**, 469 (2000).  
 4. K. H. Kaestner, D. G. Silberg, P. G. Traber, G. Schutz, *Genes Dev.* **11**, 1583 (1997).

5. O. Pabst, R. Zweigerdt, H. H. Arnold, *Development* **126**, 2215 (1999).  
 6. F. Beck, F. Tata, K. Chawengsaksophak, *Bioessays* **22**, 431 (2000).  
 7. J. P. Clatworthy, V. Subramanian, *Mech. Dev.* **101**, 3 (2001).  
 8. M. Bjerknes, H. Cheng, *Gastroenterology* **116**, 7 (1999).  
 9. V. Korinek et al., *Nature Genet.* **19**, 379 (1998).  
 10. C. Akazawa, M. Ishibashi, C. Shimizu, S. Nakanishi, R. Kageyama, *J. Biol. Chem.* **270**, 8730 (1995).  
 11. N. Ben-Arie et al., *Development* **127**, 1039 (2000).  
 12. N. A. Bermingham et al., *Neuron* **30**, 411 (2001).  
 13. X-gal staining of adult intestines was performed as described (18); for embryos, 10- $\mu$ M sections from frozen blocks of 4% paraformaldehyde-fixed intestinal tissue were stained overnight at 37°C in a pH 8.0 solution containing 1.3 mM MgCl<sub>2</sub>, 15 mM NaCl, 44 mM Hepes buffer (pH 7.3), 3 mM potassium ferricyanide, 3 mM potassium ferrocyanide and 0.05% X-gal. Sections were counterstained with nuclear fast red.  
 14. Supplementary material is available on Science Online at [www.sciencemag.org/cgi/content/full/294/5549/2153/DC1](http://www.sciencemag.org/cgi/content/full/294/5549/2153/DC1)  
 15. E. Blaugrund et al., *Development* **122**, 309 (1996).  
 16. Q. Yang, H.Y. Zoghbi, unpublished data.  
 17. Hematoxylin and eosin or Alcian blue and neutral red staining and immunohistochemistry were performed according to standard protocols. The source and final dilution of the primary antibodies were as follows: rabbit chromogranin A antibody (1:2000), gastrin antibody (1:300), glucagon antibody (1:2000), serotonin antibody (1:20000), somatostatin antibody (1:4000), neurotensin antibody (1:2500) are from DiaSorin; rabbit synaptophysin antibody (1:200, BioGenex), and rabbit Ki-67 antibody (1:1000, Novocastrol). For EM, different regions of E18.5 intestines were fixed in 3% phosphate-buffered glutaraldehyde and post fixed in phosphate-buffered osmium tetroxide. Specimens were dehydrated and embedded in

Araldite 502 resin. Semithin sections (0.4  $\mu$ M) were stained with methylene blue and basic fuchsin. Thin sections (60 nM) were stained with uranyl acetate and lead citrate. The samples were observed on a JEOL 1210 electron microscope.  
 18. T. S. Stappenbeck, J. I. Gordon, *Development* **127**, 2629 (2000).  
 19. L. Bry et al., *Proc. Natl. Acad. Sci. U.S.A.* **91**, 10335 (1994).  
 20. RNA was extracted from E18.5 intestine using TRIzol (Gibco BRL) according to manufacturer's instructions. cDNA synthesis was performed as described (28). Cryptdin and glucose-6-phosphate dehydrogenase (G6PDH) primers and PCR were as previously described (21, 25), except for the thermal cycle profile: a single denaturing step at 96°C for 1 min followed by 25 cycles of 96°C for 30 s; 55°C for 30 s; 73°C for 1 min.  
 21. D. Darmoul, D. Brown, M. E. Selsted, A. J. Ouellette, *Am. J. Physiol.* **272**, G197 (1997).  
 22. T. Ito et al., *Development* **127**, 3913 (2000).  
 23. A. Apelqvist et al., *Nature* **400**, 877 (1999).  
 24. G. Rindi et al., *Development* **126**, 4149 (1999).  
 25. J. Jensen et al., *Nature Genet.* **24**, 36 (2000).  
 26. J. L. Zheng, J. Shou, F. Guillemot, R. Kageyama, W. Gao, *Development* **127**, 4551 (2000).  
 27. T. Miyata, T. Maeda, J. E. Lee, *Genes Dev.* **13**, 1647 (1999).  
 28. J. Jensen, P. Serup, C. Karlsen, T. F. Nielsen, O. D. Madsen, *J. Biol. Chem.* **271**, 18749 (1996).  
 29. We thank S. Henning, K. Zaret, and V. Wang for thoughtful discussions; H. Bellen, B. Hassan, and M.-J. Tsai for critical reading; V. Brandt for thoughtful suggestions on the paper; T. Sudo for *Hes-1* antiserum; A. Major, J. Barrish, B. Antalffy, P. Grennan, and M. Fernandez for technical assistance; and M. Gershon for advice on the acetylcholinesterase activity assay. H.Y.Z. is an investigator of the Howard Hughes Medical Institute. Q.Y. is supported by a NASA grant.

24 August 2001; accepted 2 October 2001

## Structural Mechanisms of QacR Induction and Multidrug Recognition

Maria A. Schumacher,<sup>1</sup> Marshall C. Miller,<sup>1</sup> Steve Grkovic,<sup>2</sup> Melissa H. Brown,<sup>2</sup> Ronald A. Skurray,<sup>2</sup> Richard G. Brennan<sup>1\*</sup>

The *Staphylococcus aureus* multidrug binding protein QacR represses transcription of the *qacA* multidrug transporter gene and is induced by structurally diverse cationic lipophilic drugs. Here, we report the crystal structures of six QacR-drug complexes. Compared to the DNA bound structure, drug binding elicits a coil-to-helix transition that causes induction and creates an expansive multidrug-binding pocket, containing four glutamates and multiple aromatic and polar residues. These structures indicate the presence of separate but linked drug-binding sites within a single protein. This multisite drug-binding mechanism is consonant with studies on multidrug resistance transporters.

The emergence of multidrug resistance (MDR) has been attributed in part to membrane transport systems capable of effluxing a broad spectrum of toxic compounds (1-4).

In cancer cells, resistance to chemotherapeutic agents is mediated by the P-glycoprotein efflux pump (5, 6), whereas in bacteria MDR transporters are responsible for resistance to many clinically important antimicrobial compounds (7, 8). The serious health threat posed by the emergence of strains of antibiotic-resistant *Staphylococcus aureus* appears to have been exacerbated by plasmid-encoded MDR efflux pumps such as QacA, which confer resistance to monovalent and bivalent

<sup>1</sup>Department of Biochemistry and Molecular Biology, Oregon Health & Science University, Portland, OR 97201, USA. <sup>2</sup>School of Biological Sciences, A12, University of Sydney, Sydney NSW 2006, Australia.

\*To whom correspondence should be addressed. E-mail: [brennanr@ohsu.edu](mailto:brennanr@ohsu.edu)

## REPORTS

cationic lipophilic antiseptics and disinfectants such as quaternary ammonium compounds (QACs) (9–12). Studies on MDR transporter proteins have provided evidence for the presence of multiple, possibly overlapping, drug-binding sites within each protein (13–18). However, advances in understanding the basis of multidrug recognition has been hampered by the difficulty of performing high-resolution structural analyses on integral membrane proteins.

Structural studies on cytosolic multidrug-binding regulatory proteins provide an alternative in delineating multidrug binding mechanisms. Structures of several regulatory proteins bound to a particular drug have been determined; the *Escherichia coli* MarR repressor bound to salicylate (19), the *Bacillus subtilis* transcriptional activator BmrR bound to tetraphenylphosphonium (TPP<sup>+</sup>) and DNA (20) and the human nuclear xenobiotic receptor (PXR) bound to the cholesterol lowering drug SR12813 (21). The 23-kD *S. aureus* QacR repressor, a member of the TetR family of repressors (22), is another multidrug binding protein, which regulates the expression of the *qacA* MDR pump gene (23, 24). QacR is induced by binding mono and bivalent cationic lipophilic drugs, many of which are substrates of QacA. We report here the structures of QacR bound to six of these structurally diverse cytotoxic agents (“drugs”), rhodamine 6G (R6G), ethidium (Et), dequalinium (Dq), crystal violet (CV), malachite green (MG) and berberine (Be) (Fig. 1).

The structure of QacR bound to R6G was determined by multiple wavelength anomalous dispersion (MAD) (Fig. 2A, Table 1) [Web fig. 1, Web table 1 (25)] (26, 27). QacR is entirely helical and comprises nine helices (Fig. 2B). The first three helices form a three-helix bundle DNA binding domain, which contains a helix-turn-helix (HTH) motif ( $\alpha 2$  and  $\alpha 3$ ). Helices 4 through 9 form the drug binding/dimerization domain and formation of the dimer buries 1530 Å<sup>2</sup> of surface area per monomer. The structure reveals that QacR binds one R6G molecule per dimer (Fig. 2B). Equilibrium dialysis and Scatchard analyses [Web fig. 2 (25)] confirmed the 1:2 (drug:QacR subunit) stoichiometry (28). In contrast, the family member TetR binds two tetracycline molecules per dimer. However, the multidrug binding proteins, EmrR and BmrR, also appear to bind their ligands with a 1:2 (drug:subunit) stoichiometry (29, 30).

Comparison of the R6G-bound structure with a QacR-DNA structure determined in our lab (Fig. 2, C and D) reveals that binding of the drug triggers a coil-to-helix transition of residues Thr<sup>89</sup>-Tyr<sup>93</sup> (Fig. 2B) of the drug-bound subunit only, such that the COOH-terminus of  $\alpha 5$  is elongated by a turn; the

drug-free subunit in the dimer retains the “DNA-bound” coil structure (31) [Web fig. 1 (25)]. This transition is likely facilitated by the conversion of Tyr<sup>92</sup>, which is the only Ramachandran outlier in the drug-free state, from an unfavorable to a favorable conformation. In its unfavorable coil position, Tyr<sup>92</sup> plays an essential role in formation of the protein hydrophobic core. Upon drug binding, Tyr<sup>92</sup> is expelled from the hydrophobic core into the solvent. Tyr<sup>93</sup> is also dislodged from the hydrophobic core to a peripheral site, where it stacks with R6G (Fig. 2, C and D). Tyr<sup>92</sup> and Tyr<sup>93</sup> thus act as structural drug surrogates that stabilize the inducer-binding pocket in the absence of drug.

The coil-to-helix transition is the key not only for drug binding but also for induction as the formation of the additional turn of helix leads to the relocation of  $\alpha 6$  and its tethered DNA-binding domain (Fig. 2C). Movement of  $\alpha 6$  leads to a 9.1 Å translation and 36.7° rotation of the DNA-binding domain, relative to DNA-bound QacR (31). There is also a pendulum motion of  $\alpha 4$  upon drug binding (Fig. 2C). Concomitant structural changes, necessary for retention of interaction between the  $\alpha 6$  and  $\alpha 6'$  helices, in

the drug-free subunit of the dimer also occur. The DNA-binding domain of the drug-free subunit undergoes a 3.9 Å translation and 18.3° rotation compared to the DNA-bound conformation. Overall, there is a large increase in the center-to-center distance of the recognition helices from 37 Å (DNA-bound form) to 48 Å (drug-bound form). In contrast, in TetR there is only a 3 Å increase in the center-to-center distance of the recognition helices upon tetracycline binding (32).

The drug-binding pocket created by tyrosine expulsion is extensive and composed of residues from all helices of the inducer-binding domain except  $\alpha 9$ , as well as residues from  $\alpha 8'$  (where prime indicates the other subunit of the dimer). The portal to the aromatic ligand-binding site is formed by the divergence of  $\alpha 6$ ,  $\alpha 7$ ,  $\alpha 8$ , and  $\alpha 8'$ . Because this portal is the only apparent entry into the pocket, the structure suggests a possible explanation for the 1:2 drug:QacR stoichiometry. The COOH-terminus of  $\alpha 8$ , the intervening turn (T) and the NH<sub>2</sub>-terminus of  $\alpha 9$  are apposed to residues in the conformational switch region of  $\alpha 5$  and  $\alpha 6$  (Fig. 2C), and thus the drug induced coil-to-helix transition forces the movement of  $\alpha 8$ -T- $\alpha 9$  into

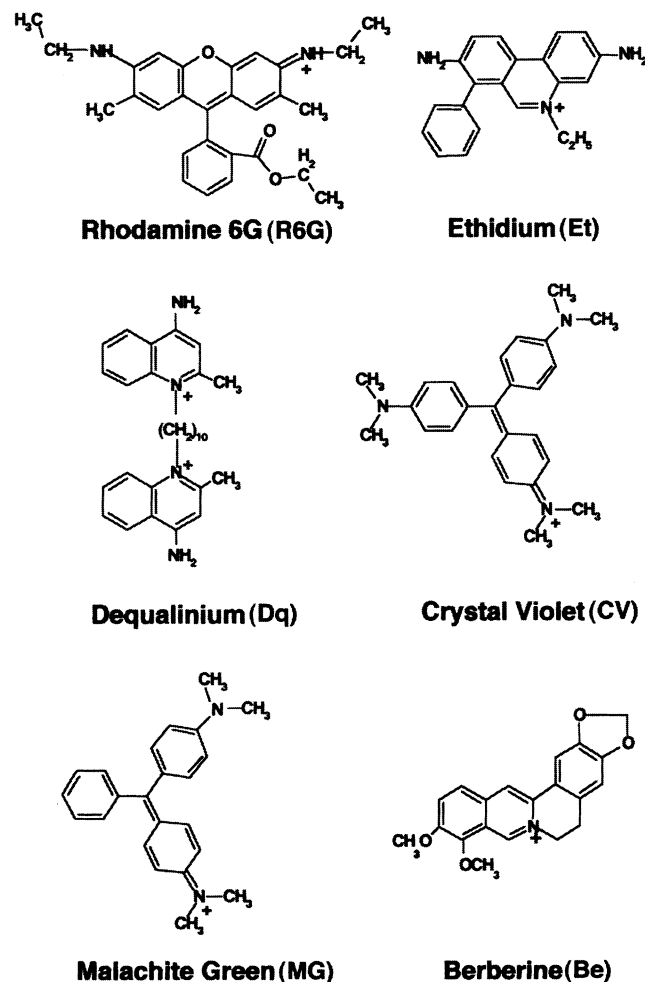


**Fig. 1.** The chemical structures of six cationic lipophilic drugs bound by QacR that were used in this study. The positively charged nitrogens are indicated. Note the bivalent nature of the inducer, dequalinium.

the drug-binding pocket of the neighboring subunit, limiting access to its entrance.

Within the drug-binding pocket, the three-ring system of R6G is wedged between Trp<sup>61</sup> from  $\alpha 4$  and Tyr<sup>93</sup> from  $\alpha 5$  (Fig. 3A). The phenyl moiety makes hydrophobic interactions with Tyr<sup>123</sup> and Leu<sup>54</sup>, whereas its oxygen moiety, O27A, hydrogen bonds to a water molecule. Additional water molecules fill the portion of the large drug-binding pocket that is unoccupied by drug. Asparagine, glutamine, threonine, and serine residues in the pocket provide versatility for contacting polar moieties of different drugs. In the QacR-R6G complex, Gln<sup>96</sup> contacts the R6G N1 atom and Gln<sup>64</sup> and Thr<sup>89</sup> contact the R6G N2. The R6G ring system is further anchored by an interaction between the central ring O1 atom and the O $\gamma$  of Thr<sup>89</sup>.

A distinguishing feature of multidrug binding proteins that recognize cationic drugs appears to be the presence of buried negatively charged glutamates or aspartate residues. This was clearly demonstrated in the BmrR-TPP<sup>+</sup>-DNA structure, which contains a buried glutamate, Glu<sup>253</sup>, critical for drug binding (20). In the QacR drug-binding site there are four glutamate residues, Glu<sup>57</sup> and Glu<sup>58</sup> from  $\alpha 4$ , Glu<sup>90</sup> from  $\alpha 5$ , and Glu<sup>120</sup> from  $\alpha 7$ , all of which are partially buried and surround the drug-binding pocket. In the QacR-R6G complex, Glu<sup>90</sup> neutralizes the positively charged ethyl ammonium group of the drug (Fig. 1). Glu<sup>90</sup> is also part of the conformational switch region of  $\alpha 5$  and is translocated into the drug-binding pocket only upon drug binding.

All QacR-drug structures described in this study (Fig. 1 and Table 1) utilize the identical induction mechanism. In the QacR-Et structure the Et is bound in a pocket that is distinct but partially overlaps that of the R6G binding site (compare Fig. 3, A and B). The “Et pocket” is closer to the proposed “portal” entrance than the “R6G pocket,” yet the phenanthridinium ring system of the Et is adequately inserted to elicit the tyrosine expulsion process and thus, flip the induction switch. Unlike the R6G complex, the formal positive charge on the Et (Fig. 1) is not complemented by Glu<sup>90</sup>, but by Glu<sup>120</sup> (27). Two aromatic residues, Tyr<sup>103</sup> and Phe<sup>162</sup>, sandwich the phenanthridinium system and additional stacking interactions, including those between Tyr<sup>123</sup> and the ethidium exocyclic 6-phenyl moiety, secure the Et (Fig. 3B). The most buried phenanthridinium phenyl group is wedged between Ile<sup>99</sup> and Ile<sup>100</sup> from  $\alpha 6$ , while its N1 amino group nitrogen is hydrogen bonded to the O $\epsilon 2$  of Gln<sup>96</sup>. As in the QacR-R6G, several solvent molecules occupy the void in the pocket that is not filled by drug.

The volume of the drug-binding pocket, which has dimensions of  $\sim 10$  Å by 9 Å by 23

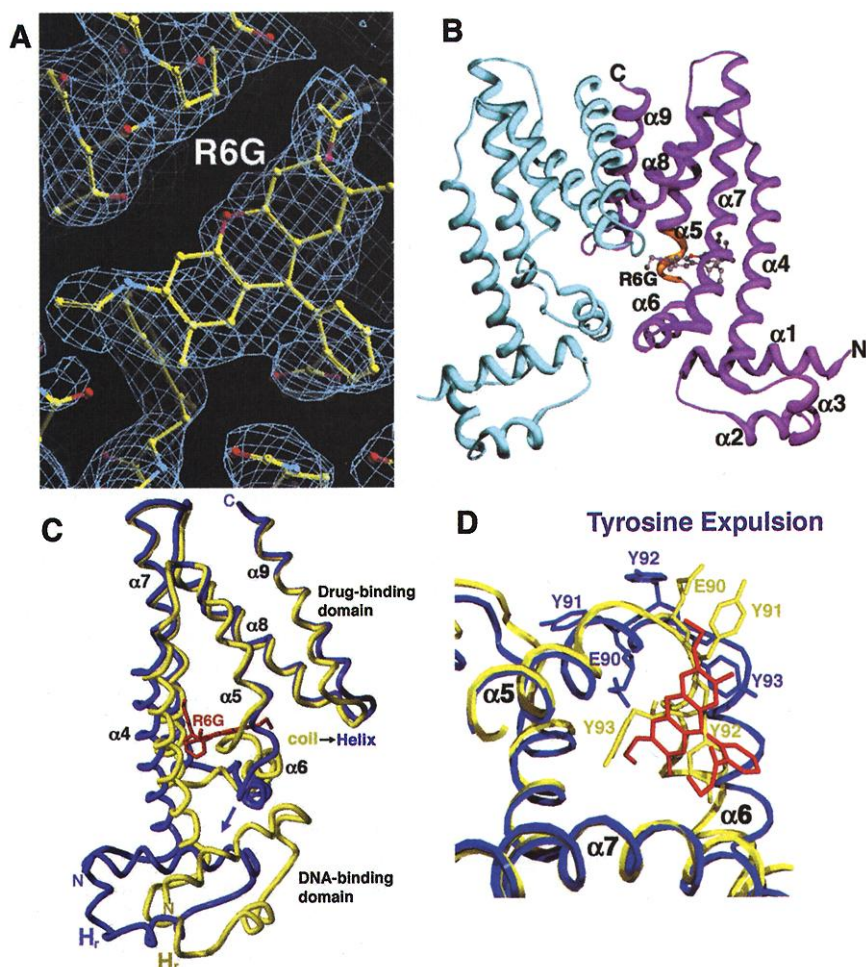


**Fig. 2.** The mechanism of multidrug binding and induction. (A) Simulated annealing omit map of the R6G drug-binding pocket. Composite electron density omit map (contoured at 1.5  $\sigma$ ) calculated with a starting temperature of 2000 K and excluding R6G from the model. Carbon, nitrogen, and oxygen atoms are colored yellow, light blue, and red, respectively. (B) Structure of the drug-bound QacR-R6G complex. QacR consists of nine helices:  $\alpha 1$ (3-18),  $\alpha 2$ (25-32),  $\alpha 3$ (36-42),  $\alpha 4$ (46-71),  $\alpha 5$ (75-88; 75-93 in the drug-bound subunit, see below),  $\alpha 6$ (96-108),  $\alpha 7$ (110-136),  $\alpha 8$ (145-162), and  $\alpha 9$ (168-185). The yellow region (residues 89 to 93) forms a helix upon drug binding. The bound R6G is shown as balls and sticks with carbon, oxygen, and nitrogen colored gray, red, and blue, respectively. (C) Superimposition of the core drug-binding region, residues 55 to 188, of the DNA-bound conformation (yellow) onto the drug-bound conformation (blue) revealing the structural changes that occur upon drug binding. R6G is depicted as a red stick model. The DNA-binding recognition helix is labeled H<sub>r</sub>. (D) Close-up view of the R6G binding pocket before (yellow) and after (blue) drug binding depicting the drug-induced tyrosine expulsion of Tyr<sup>92</sup> and Tyr<sup>93</sup> from the core and concomitant coil-to-helix transition in which residues 89 to 93 are incorporated into  $\alpha 5$ , thus lengthening it by one turn.

Å, is 1100 Å<sup>3</sup> as determined by the program “putative active sites with spheres” (PASS) (33), whereas the largest pocket of drug-free QacR is under 400 Å<sup>3</sup> (Fig. 4, A and B). When PASS was used to search for potential ligand binding within the drug-removed QacR structure, the top two predicted binding sites, which have overlapping volumes, correspond to the centers of the Et and the R6G drug-binding pockets (Fig. 4A) (33). This computational analysis, therefore, provides additional unbiased support for the presence of two separate but potentially overlapping binding sites within a single pocket. In addition to binding monovalent lipophilic cations, QacR also binds bivalent cationic lipophilic

compounds, e.g., dequalinium (Dq). The 2.54 Å resolution structure of the QacR-Dq complex reveals that the two positively charged aminomethylquinolinium moieties bind the pockets defined as the R6G pocket and the Et pocket, while the decamethylene linker adjusts to provide an optimal fit (Fig. 3C and Fig. 4A). In the R6G pocket, one quinolinium group is sandwiched between Trp<sup>61</sup> and Tyr<sup>93</sup>, similar to R6G binding. However, unlike R6G, the positively charged nitrogen of this moiety (Fig. 1) is complemented by Glu<sup>57</sup> and Glu<sup>58</sup>. In the Et pocket, the Dq contacts are functionally identical to those observed in the QacR-Et complex; the second quinolinium group is bound between Phe<sup>162</sup>

**Fig. 3.** Multidrug recognition by QacR. For the sake of clarity, only key residues are shown (no solvent) including the acidic residues (colored red) that neutralize the positive charges of each drug. The carbon, nitrogen, and oxygen atoms of the drugs are colored white, blue, and red, respectively. (A) QacR-R6G complex. (B) QacR-Et complex. (C) QacR-Dq complex. (D) QacR-CV complex. (E) QacR-MG complex. (F) QacR-Be complex. The distances between the positively charged nitrogens of each drug and QacR acidic residues are: R6G [Oε2(Glu<sup>90</sup>)-N1(R6G), 3.98 Å]; Et: [Oε2(Glu<sup>120</sup>)-N2(Et), 3.95 Å]; Dq: [Oε1(Glu<sup>57</sup>)-N2(Dq), 4.75 Å; Oε1(Glu<sup>58</sup>)-N2(Dq), 4.93 Å; and Oε1(Glu<sup>120</sup>)-N1(Dq), 4.80 Å]; CV: [Oε1(Glu<sup>90</sup>)-N2(CV), 3.96 Å; Oε2(Glu<sup>120</sup>)-N3(CV), 3.85 Å]; MG: [Oε1(Glu<sup>90</sup>)-N2(MG), 3.35 Å; Oε2(Glu<sup>120</sup>)-N3 (MG), 3.60 Å]; Be: [Oε1(Glu<sup>57</sup>)-N1(Be), 5.64 Å; Oε1(Glu<sup>58</sup>)-N1(Be), 4.93 Å].

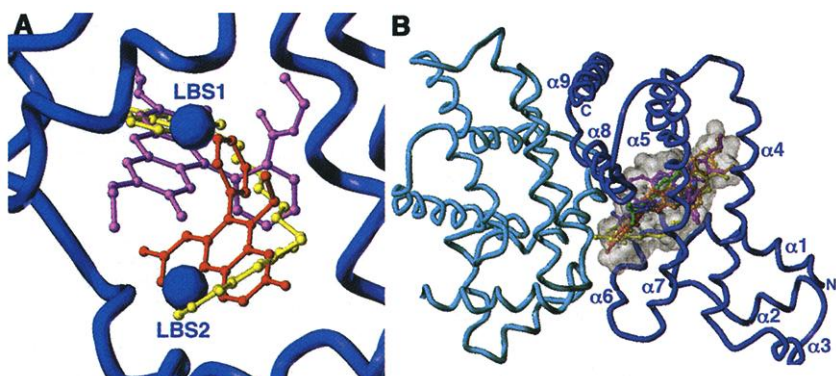
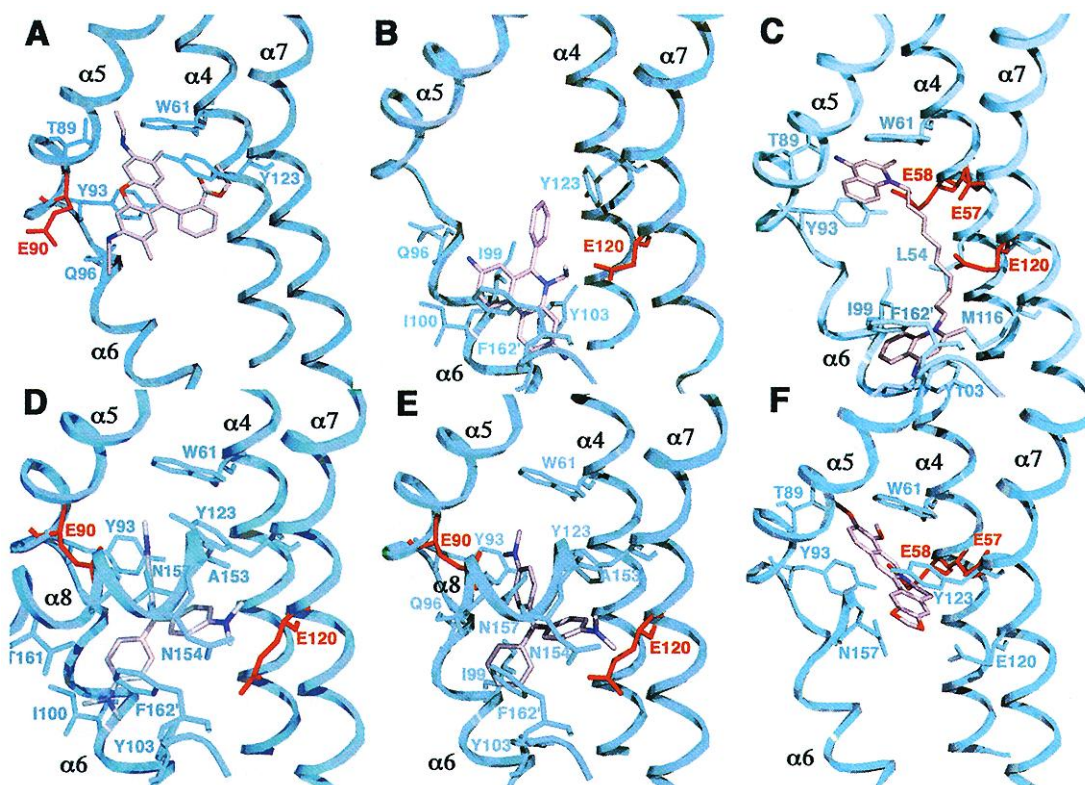


**Fig. 4.** The extended multisite binding pocket of QacR. (A) Superimposition of drug-binding pockets of the QacR-R6G, QacR-Et, and QacR-Dq complexes highlighting the multisite binding pocket of QacR. R6G, Et, and Dq are colored pink, orange, and yellow, respectively. The two top binding-site centers predicted from PASS (33) are depicted as blue balls and labeled ligand binding site 1 and 2 (LBS1 and LBS2). (B) Ribbon diagram of the drug-bound QacR dimer looking down from the "top" of the dimer. The drug-bound subunit is colored dark blue and the other is cyan. The binding-site volume calculated from PASS with drugs removed is depicted as a transparent surface. Shown within this volume as sticks are the drugs from all structures where R6G is pink, Et is orange, Dq is light yellow, MG is green, CV is violet, and Be is dark yellow. Note the optimal fit of the drugs within the extended binding site. The helices in the drug-bound protomer are labeled.

and Tyr<sup>103</sup>, and its positively charged nitrogen is neutralized by Glu<sup>120</sup> (Fig. 3C). The decamethylene linker is well ordered and makes multiple van der Waals contacts with the side chains of Leu<sup>54</sup>, Ile<sup>99</sup>, Met<sup>116</sup>, and Leu<sup>119</sup>.

Unlike R6G, Et and Dq, the QacR inducer crystal violet (CV) (21) does not have a planar ring system (Fig. 1). Instead, this dye has a propeller-like geometry with dihedral angles between aryl groups and the central coordination plane of 27.7° (34). As a result,

CV should not be able to sandwich into either the R6G or the Et binding pockets of QacR. The structure of the QacR-CV complex reveals that, somewhat like Dq, CV binds in the overlapping region between the R6G and Et pockets such that its aryl groups interact with hydrophobic residues at the edges of each pocket (Fig. 3D). Specifically, the methyl groups of one dimethylaminophenyl moiety make hydrophobic interactions with Tyr<sup>93</sup> and Trp<sup>61</sup> near the R6G binding site, whereas its phenyl group stacks against Tyr<sup>123</sup>. The

methyl and phenyl groups of a second dimethylaminophenyl moiety are within van der Waals distance of Tyr<sup>103</sup> and Phe<sup>162</sup>, i.e., near the Et pocket. The CV methyl groups also engage in hydrophobic interactions with Ile<sup>100</sup> and Ile<sup>100'</sup>. Finally, the third dimethylaminophenyl moiety is anchored to a pocket between α7 and α8 where it contacts Ala<sup>153</sup>, Glu<sup>120</sup>, Asn<sup>154</sup>, and Asn<sup>157</sup>. This unique binding mode allows the dissipation of the delocalized positive charge of CV (Fig. 1) via interactions between two of its amino groups and glutamates, Glu<sup>90</sup> and Glu<sup>120</sup>.

From the manner in which the delocalized charge of CV is neutralized by Glu<sup>90</sup> and Glu<sup>120</sup>, we predicted that replacement of the third dimethyl amino group with a hydrogen, as found in malachite green (MG), although removing several hydrophobic contacts, should not prevent binding. Indeed, the QacR-MG structure demonstrates that this dye binds in essentially the same pocket as CV, and its positive charge is similarly complemented as in CV (Fig. 3E). However, superimposition of the QacR CV and MG complexes reveals a slight shift in the position of one drug relative to the other, allowing each to make optimal van der Waals contacts with QacR residues, again underscoring the versatility of the pocket. Although MG binds QacR, whether it is a physiologically relevant inducer of *qacA* is unknown.

The plant alkaloid, berberine (Be), is a substrate of QacA that induces QacR and is a potent antimicrobial in the absence of MDR transporters (35, 36). Be binds within the

**Table 1.** QacR-drug complex data collection and refinement.

Parameter	Drug					
	R6G (remote/seleno)	Et	Dq	CV	MG	Be
<i>Data collection statistics</i>						
Temperature (K)	100	100	100	100	296	296
Space group	P4 <sub>2</sub> ,2 <sub>1</sub> ,2					
Cell constants (Å)	a=172.3 b=172.3 c=95.0	a=172.0 b=172.0 c=95.0	a=172.0 b=172.0 c=94.6	a=172.9 b=172.9 c=95.1	a=174.2 b=174.2 c=96.3	a=174.3 b=174.3 c=96.3
Resolution (Å)	2.84	2.97	2.54	2.85	2.95	2.98
Completeness (%)	99.8	75.0	99.6	100.0	86.8	92.7
Overall <i>R</i> <sub>sym</sub> (%)*	4.9	4.5	5.8	6.4	8.9	10.5
Multiplicity	6.9	6.0	7.1	9.9	4.0	4.1
Overall <i>I</i> /σ( <i>I</i> )	10.5	12.0	9.0	8.5	11.0	10.2
Total reflections (#)	236,668	130,105	391,013	340,448	81,820	141,045
Unique reflections (#)	34,367	22,060	55,291	34,304	26,915	32,199
High res. shell (Å)	2.91–2.84	3.15–2.97	2.61–2.54	2.92–2.85	3.10–2.95	3.05–2.98
<i>R</i> <sub>sym</sub> (%)	25.9	22.9	34.2	44.9	27.8	25.2
<i>I</i> /σ( <i>I</i> )	2.9	3.0	2.1	1.7	2.4	2.2
<i>Refinement statistics</i>						
Resolution range (Å)						
Low	77.06	83.16	86.00	63.97	64.60	84.29
High	2.84	2.97	2.54	2.85	2.95	2.98
<i>R</i> <sub>work</sub> (%)†	22.9	23.8	20.9	22.8	23.7	23.6
<i>R</i> <sub>free</sub> (%)‡	27.2	28.9	25.5	28.6	28.1	28.4
rmsd						
Bond angles (°)	1.30	1.31	1.61	1.44	1.65	1.60
Bond lengths (Å)	0.009	0.009	0.014	0.011	0.015	0.014
B values (Å <sup>2</sup> )	1.59	1.55	2.88	2.43	1.43	1.43
Solvent	66/23	51/17	137/24	68/24	7/22	7/22
[ (#), water/sulfate ]						
Ramachandran analysis						
Most favored (%)	89.9	82.9	90.9	87.4	84.8	85.9
Additionally allowed (%)	9.7	15.9	7.6	11.9	14.1	12.6
Generously allowed (%)	0.0	0.7	0.9	0.4	0.4	0.9
Disallowed (%)	0.4	0.6	0.7	0.4	0.7	0.7

\**R*<sub>sym</sub> = ΣΣ|*I*<sub>hkl</sub> - *I*<sub>hkl</sub>(*j*)|/Σ*I*<sub>hkl</sub>, where *I*<sub>hkl</sub>(*j*) is observed intensity and *I*<sub>hkl</sub> is the final average value of intensity.  
†*R*<sub>work</sub> = Σ||*F*<sub>obs</sub> - *F*<sub>calc</sub>||/Σ|*F*<sub>obs</sub>|    ‡*R*<sub>free</sub> = Σ||*F*<sub>obs</sub> - *F*<sub>calc</sub>||/Σ|*F*<sub>obs</sub>|, where all reflections belong to a test set of 10% data randomly selected in CNS.

R6G pocket of QacR (Fig. 3F), and like R6G, the Be anthracene ring system is sandwiched between Trp<sup>61</sup> and Tyr<sup>93</sup> while the 1,3-dioxo-6a-azoniaindeno group stacks with Tyr<sup>123</sup> and is anchored by hydrogen bonds from its 1,3 oxygens to Asn<sup>157</sup>. At the other end of the ring system, the two 8,9-dimethoxy groups extend into a solvent exposed region, which is formed when the coil-to-helix transitional switch is thrown. Finally, the positive charge, centered on the Be N1 nitrogen (Fig. 1), is surrounded by the side chains of Glu<sup>57</sup> and Glu<sup>58</sup> in a manner analogous to that observed for one of the aminomethylquinolinium nitrogens in the QacR-Dq structure.

In conclusion, QacR exhibits an expansive drug-binding site with four charge-neutralizing residues that line and surround the pocket. There is a large number of aromatic residues and several polar residues in the pocket that can act in a drug-specific manner as either hydrogen bond donors or acceptors. The importance of polar residues for multidrug recognition was demonstrated by the PXR-SR12813 structure in which multiple orientations of the SR12813 ligand were ob-

served within its large binding pocket, and stabilized by a different complement of polar residues (21). In addition, the recent structure of the *E. coli* MsbA, a homolog of the multidrug ABC transporters, revealed a large putative ligand binding cavity lined by polar residues (37). Finally, the combined QacR-drug structures reveal several, separate, but linked binding sites within one extended and thus, multifaceted drug binding pocket. This is likely to be a crucial feature in multidrug recognition. Indeed, the use of such a multifaceted pocket is consistent with accumulating data indicating the presence of multiple binding sites in both secondary and ATP-dependent multidrug transporters (13–18).

**References and Notes**

1. S. Levy, *Antimicrob. Agents Chemother.* **36**, 695 (1992).
2. H. Nikaido, *Science* **264**, 382 (1994).
3. M. M. Gottesman, I. Pastan, S. V. Ambudkar, *Genet. Dev.* **6**, 610 (1996).
4. S. V. Ambudkar et al., *Annu. Rev. Pharmacol. Toxicol.* **39**, 361 (1999).
5. T. Licht, I. Pastan, M. M. Gottesman, F. Hermann, *Ann. Hematol.* **72**, 184 (1996).

6. L. J. Goldstein, I. Pastan, M. M. Gottesman, *Crit. Rev. Oncol. Hematol.* **12**, 243 (1992).
7. M. Putman, H. W. van Veen, W. N. Konings, *Microbiol. Mol. Biol. Rev.* **64**, 672 (2000).
8. I. T. Paulsen, M. H. Brown, R. A. Skurray, *Microbiol. Rev.* **60**, 575 (1996).
9. J. M. Tennent et al., *J. Gen. Microbiol.* **135**, 1 (1989).
10. M. H. Brown, R. A. Skurray, *J. Mol. Microbiol.* **3**, 163 (2001).
11. H. Behr et al., *Pathol. Biol.* **42**, 438 (1994).
12. S. Mayer, M. S. Boos, A. Beyer, A. C. Fluit, F. J. Schmitz, *J. Antimicrob. Chemother.* **47**, 869 (2001).
13. M. Putman, L. A. Koole, H. W. van Veen, W. N. Konings, *Biochemistry* **38**, 13900 (1999).
14. M. Kolaczowski et al., *J. Biol. Chem.* **271**, 31543 (1996).
15. H. W. van Veen et al., *Nature* **391**, 291 (1998).
16. B. A. Mitchell, I. T. Paulsen, M. H. Brown, R. A. Skurray, *J. Biol. Chem.* **274**, 3541 (1999).
17. I. T. Paulsen, M. H. Brown, T. G. Littlejohn, B. A. Mitchell, R. A. Skurray, *Proc. Natl. Acad. Sci. U.S.A.* **93**, 3630 (1996).
18. L. Tamai, A. R. Safa, *J. Biol. Chem.* **266**, 16796 (1991).
19. M. N. Alekshun, S. B. Levy, T. R. Mealy, B. A. Seaton, J. F. Head, *Nature Struct. Biol.* **8**, 710 (2001).
20. E. E. Heldwein, R. G. Brennan, *Nature* **409**, 378 (2001).
21. R. E. Watkins et al., *Science* **292**, 2329 (2001).
22. H. Aramaki, N. Yagi, M. Suzuki, *Protein Eng.* **8**, 1259 (1995).
23. S. Grkovic, M. H. Brown, N. J. Roberts, I. T. Paulsen, R. A. Skurray, *J. Biol. Chem.* **273**, 18665 (1998).
24. S. Grkovic et al., *J. Bacteriol.* **183**, 7102 (2001).
25. Supplementary material is available on Science Online at [www.sciencemag.org/cgi/content/full/294/5549/2158/DC1](http://www.sciencemag.org/cgi/content/full/294/5549/2158/DC1)
26. W. A. Hendrickson, *Science* **254**, 51 (1991).
27. The COOH-terminally hexa-histidine tagged C72A/C141S QacR protein, which retains wild-type DNA and drug-binding activity (24), was overexpressed and purified as described (23, 24). To crystallize the QacR-drug complexes reproducibly, the protein was subjected to reductive alkylation of lysines as described by Rayment (38). The alkylation reaction is terminated by addition of glycine to a final concentration of 200 mM and the protein is concentrated to 15 mg/ml and buffer exchanged into 25 mM Tris (pH 7.5), 50 mM imidazole, 300 mM NaCl, and 5% glycerol. Drug-binding studies reveal that the alkylated protein binds R6G with normal affinity (~150 nM compared to unalkylated protein of 101 ± 4 nM). Crystals of the QacR-drug complexes were obtained by using 10 to 150 μM drug and 3 M ammonium sulfate. The crystals are tetragonal, P4<sub>2</sub>,2<sub>1</sub>,2, with a = b = 172.0 Å and c = 94.6 Å. One small isomorphous QacR-Et crystal has been grown without alkylation, but its diffraction was limited to 3.7 Å resolution. Attempts to solve the QacR-R6G structure by molecular replacement using the DNA-bound QacR structure failed and multiple wavelength anomalous dispersion (MAD), using selenomethionine-substituted (seleno) QacR, was used. The seleno-QacR protein was expressed as described (39) and the protein purified and crystallized with drug as for the wild-type protein except 1 mM β-mercaptoethanol was added to all solutions. The crystals are cryoprotected with solutions of 3 M ammonium sulfate, 40% glycerol. MAD diffraction data were collected at SSRL beamline 9-2 at 100 K and processed with MOSFLM as were data for the QacR-Et complex. Data for QacR-CV and QacR-Dq crystals were collected at SSRL beamline 11-1 at 100 K and processed with MOSFLM. Data for the QacR-MG and QacR-Be complexes were collected at room temperature with an R-Axis IV imaging plate system and processed with BIOTEX. Using SOLVE (40), six selenium sites were located using the MAD QacR-R6G data. The two remaining sites were found by difference Fourier methods. The MAD parameters were refined, phases calculated and density modification carried out in CNS (41) [Web table 1 (25)]. The solvent-flipped map was of superb quality, allowing the complete trace (42) of both QacR dimers in the ASU. One dimer contains one R6G molecule, the other dimer is drug-free (43). Multiple cycles of SA/positional/thermal parameter refinement were carried out in CNS (41) and rebuilding was done in O (42). The final *R*<sub>work</sub> is 22.9% and the *R*<sub>free</sub> is 27.2% using all data

to 2.84 Å. The model has excellent stereochemistry (44) (Table 1). The final model (for each QacR-drug complex) includes the drug and residues 2 to 187 of each subunit as well as several sulfate molecules that are associated with residues from the DNA binding domains (Table 1). CNS drug topology and parameter files were obtained using the HIC-Up-server at ([http://xray.bmc.uu.se/cgi-bin/gerard/hicup\\_server.pl](http://xray.bmc.uu.se/cgi-bin/gerard/hicup_server.pl)). The remaining QacR-drug complexes were prepared and crystallized similarly and their structures are isomorphous with the QacR-R6G structure (Table 1). In each case, the starting QacR model, with drug removed, was subjected to rigid body refinement in CNS followed by SA/positional/thermal parameter refinement. Composite omit maps showing the region around each drug are in Supplementary fig. 3. Relevant intensity data collection, refinement statistics, and resolution limits for all QacR complexes are listed in Table 1. In all QacR-drug complexes Tyr<sup>92</sup> of the drug-free subunits is a Ramachandran outlier as is, in some cases, Lys<sup>44</sup> of the DNA binding domain, which has weak density. Figure 2, B to D, and Fig. 3, A to F, were generated with Swiss PDB Viewer (45) and rendered with POV-Ray (46). Figure 4, A and B, was generated using Sybyl6.7. Figure 2A was made with O (42).

28. The QacR-R6G equilibrium dialysis experiments were carried out in buffer A [100 mM Hepes (pH 7.5), 250 mM potassium glutamate, 150 mM NaCl, 10 mM MgOAc, 0.5 mM EDTA, and 5% glycerol]. One-milliliter solutions of QacR dimer (400 nM) were dialyzed against 500 ml buffer A containing 75, 110, 150, or 190 nM R6G for 5 days at 4°C with stirring. After dialysis the samples were incubated at 95°C for 5 min (to denature the protein), centrifuged (14,000 rpm for 20 s), and the supernatants measured for R6G fluorescence ( $\lambda_{ex}$  520 nm,  $\lambda_{em}$  551 nm). The R6G concentrations in each dialyzed sample and its respective dialysate were quantified by transforming their fluorescence signals with a linear fit to a serial dilution of R6G in buffer A measured in identical fashion. The concentration of "bound" R6G in the QacR containing samples was determined by subtracting the concentration of "free" R6G in a dialyzed blank (Supplementary fig. 2). Control dialysis experiments included the addition of purine repressor (100 nM dimer) or BSA (100 nM) to the QacR solution (as well as their independent testing) and had no effect on QacR-R6G binding affinity.
29. M. Ahmed, C. M. Borsch, S. S. Taylor, N. Vazquez-Laslop, A. A. Neyfakh, *J. Biol. Chem.* **269**, 28506 (1994).
30. A. Brooun, J. J. Tomashek, K. Lewis, *J. Bacteriol.* **181**, 5131 (1999).
31. M. Schumacher *et al.*, unpublished data.
32. P. Orth, D. Schnappinger, W. Hillen, W. Saenger, W. Hinrichs, *Nature Struct. Biol.* **7**, 215 (2000).
33. G. P. Brady Jr., P. F. W. Stouten, *J. Computer-Aided Mol. Des.* **14**, 383 (2000).
34. S. Lovell, B. J. Marquardt, B. Kahr, *J. Chem. Soc. Perkin Trans. 2*, 2241 (1999).
35. K. Lewis, *J. Mol. Microbiol. Biotechnol.* **3**, 247 (2001).
36. S. Grkovic, M. H. Brown, R. A. Skurray, unpublished data.
37. G. Chang, C. B. Roth, *Science* **293**, 1793 (2001).
38. I. Rayment, *Methods Enzymol.* **276**, 176 (1999).
39. S. Doublé, *Methods Enzymol.* **276**, 523 (1999).
40. T. C. Terwilliger, J. Berendzen, *Acta Crystallogr. D.* **55**, 849 (1999).
41. A. T. Brünger *et al.*, *Acta Crystallogr. D* **54**, 905 (1998).
42. T. A. Jones, J.-T. Zou, S. W. Cowan, M. Kjeldgaard, *Acta Crystallogr. A* **47**, 110 (1991).
43. M. A. Schumacher *et al.*, unpublished data.
44. R. A. Laskowski, M. W. MacArthur, J. M. Thornton, *J. Appl. Crystallogr.* **26**, 283 (1993).
45. N. Guex, M. C. Peitsch, Swiss PDB, *Electrophoresis* **18**, 2714 (1997).
46. POV-Ray, Persistence of Vision Raytracer, version 3.1 ([www.povray.org](http://www.povray.org)).
47. M.A.S. is a Burroughs Wellcome Career Development Awardee. S.G. was the recipient of an Australian Postgraduate Award. Supported by grants AI 48593 from the NIH to R.G.B. and project grant 153818 from the National Health and Medical Research Council (Australia) to R.A.S. Intensity data collected at the Stanford Synchrotron Radiation Laboratory

(SSRL) was carried out under the auspices of the SSRL biotechnology program, which is supported by the NIH, National Center for Research Resources, Biomedical Technology Program, and by the Department of Energy, Office of Biological and Environmental Research. Coordinates and structure factors have

been deposited with the Protein Data Bank (Accession codes for the QacR-R6G, QacR-Et, QacR-Dq, QacR-CV, QacR-MG, and QacR-Be complexes are 1JUS, 1JTY, 1JTG, 1JTX, 1JUP, and 1JUM, respectively).

5 September 2001; accepted 26 October 2001

## Structural Basis for Selective Recognition of Oligosaccharides by DC-SIGN and DC-SIGNR

Hadar Feinberg,<sup>1</sup> Daniel A. Mitchell,<sup>2</sup> Kurt Drickamer,<sup>2</sup> William I. Weis<sup>1\*</sup>

Dendritic cell specific intracellular adhesion molecule-3 (ICAM-3) grabbing nonintegrin (DC-SIGN), a C-type lectin present on the surface of dendritic cells, mediates the initial interaction of dendritic cells with T cells by binding to ICAM-3. DC-SIGN and DC-SIGNR, a related receptor found on the endothelium of liver sinusoids, placental capillaries, and lymph nodes, bind to oligosaccharides that are present on the envelope of human immunodeficiency virus (HIV), an interaction that strongly promotes viral infection of T cells. Crystal structures of carbohydrate-recognition domains of DC-SIGN and of DC-SIGNR bound to oligosaccharide, in combination with binding studies, reveal that these receptors selectively recognize endogenous high-mannose oligosaccharides and may represent a new avenue for developing HIV prophylactics.

Initiation of a primary immune response requires the interaction of resting T cells with antigen-presenting dendritic cells (1). Initial interaction of T cells with dendritic cells is

mediated by the binding of the T cell surface receptor ICAM-3 to a dendritic cell surface receptor denoted DC-SIGN (2). DC-SIGN may also mediate rolling of dendritic cells

**Table 1.** Data collection and refinement statistics. Unit cell parameters are from postrefinement in SCALEPACK (20). Ramachandran plot regions are defined in PROCHECK (27).

	DC-SIGN	DC-SIGNR
Space group	C2	P2 <sub>1</sub> 2 <sub>1</sub> 2 <sub>1</sub>
Unit cell parameters		
a (Å)	106.8	50.2
b (Å)	148.2	57.0
c (Å)	113.0	89.3
$\beta$ (°)	91.0	
Resolution range (Å)	50 to 2.5 (2.59 to 2.50)	50 to 1.9 (1.97 to 1.90)
Measured reflections	250720	843434
Unique reflections	59357	19033
Completeness (%)	97.8(99.3)	92.0(83.6)
$R_{sym}^*$ (%)	5.3(26.6)	7.2(13.1)
$R_{crist}^\dagger$ (%)	21.4	19.4
$R_{free}^\ddagger$ (%)	25.8	24.0
Rmsd from ideality		
Bonds (Å)	0.0067	0.0049
Angles (°)	1.3	1.2
Ramachandran plot		
% in most favored	87.2	89.0
% in allowed	11.7	10.5
% generous regions	1.1	0.4
% disallowed	0.0	0.0
Average B-factor (Å <sup>2</sup> )		
Main chain	47.3	24.0
Side chain	48.7	26.2
Carbohydrate	43.2	35.5
Ca <sup>2+</sup>	40.8	17.1
Water molecules	41.9	32.6

\* $R_{sym} = \sum_h \sum_i (|I_i(h)| - \langle I(h) \rangle) / \sum_h \sum_i I_i(h)$  where  $I_i(h)$  = observed intensity, and  $\langle I(h) \rangle$  = mean intensity obtained from multiple measurements.  $^\dagger R_{crist} = \sum |F_o| - |F_c| / \sum |F_o|$ , where  $|F_o|$  = observed structure factor amplitude and  $|F_c|$  = calculated structure factor amplitude for the working and test sets, respectively.